

AD A 088905

REPORT DOCUMENTATION PAGE		READ INSTRUCTIONS BEFORE COMPLETING FORM
1. REPORT NUMBER NRL Memorandum Report 4322	2. GOVT ACCESSION NO. AD A088 905	3. RECIPIENT'S CATALOG NUMBER
4. TITLE (and Subtitle) ANALYSIS OF PROTON TRANSPORT EXPERIMENTS		5. TYPE OF REPORT & PERIOD COVERED Interim report on a continuing NRL problem.
		6. PERFORMING ORG. REPORT NUMBER
7. AUTHOR(s) F.C. Young, F.L. Sandel*, S.J. Stephanakis, P.G. Blauner*, G. Cooperstein, S.A. Goldstein*, and D. Mosher		8. CONTRACT OR GRANT NUMBER(s)
9. PERFORMING ORGANIZATION NAME AND ADDRESS Naval Research Laboratory Washington, D.C. 20375		10. PROGRAM ELEMENT, PROJECT, TASK AREA & WORK UNIT NUMBERS 67-0879-0-0
11. CONTROLLING OFFICE NAME AND ADDRESS Department of Energy Washington, D.C. 20545		12. REPORT DATE September 5, 1980
		13. NUMBER OF PAGES 34
14. MONITORING AGENCY NAME & ADDRESS (If different from Controlling Office) Sandia Laboratories Albuquerque, New Mexico 87115		15. SECURITY CLASS. (of this report) UNCLASSIFIED
		15a. DECLASSIFICATION/DOWNGRADING SCHEDULE
16. DISTRIBUTION STATEMENT (of this Report) Approved for public release; distribution unlimited.		
17. DISTRIBUTION STATEMENT (of the abstract entered in Block 20, if different from Report)		
18. SUPPLEMENTARY NOTES *Present address: JAYCOR, Inc., Alexandria, VA 22304		
19. KEY WORDS (Continue on reverse side if necessary and identify by block number) Intense proton beam Prompt-gamma diagnostic Ion transport Beam-plasma interaction Ion focusing		
20. ABSTRACT (Continue on reverse side if necessary and identify by block number) Intense 1-MeV proton beams, produced with the GAMBLE II generator at the Naval Research Laboratory, have been transported efficiently over a distance of one meter in a wall-stabilized, current carrying plasma channel. Ion beams from a pinch-reflex-diode were ballistically focused in a neutral-gas background so that a current-neutralized beam was injected into the plasma channel. Channels with diameters of 1.6 cm and 4.5 cm have been studied for gas pressures ranging from 0.1 to 1.5 Torr. Proton currents in the channels were diagnosed with absolutely calibrated prompt-gamma detectors using the $^{19}\text{F}(p,\gamma)^{16}\text{O}$ reaction. Temporal measurements are compared with calculated prompt-gamma responses to provide proton energy losses, proton currents and (Abstract continues)		

DD FORM 1473
1 JAN 73EDITION OF 1 NOV 65 IS OBSOLETE
S/N 0102-LF-014-6601

1 SECURITY CLASSIFICATION OF THIS PAGE (When Data Entered)

20. (Abstract continued)

transport efficiencies. For the small diameter channel, poor transport was observed. For the large diameter channel, efficient transport (33%-100%) was deduced for peak proton currents of ~ 0.3 MA and for energy losses of a few hundred keV.

TABLE OF CONTENTS

	<u>PAGE</u>
I. INTRODUCTION	1
II. DESCRIPTION OF EXPERIMENT	1
III. LARGE-TRANSPORT-CHANNEL RESULTS	3
IV. TRANSPORT EFFICIENCIES AND ENERGY LOSSES IN THE LARGE CHANNEL	4
V. SMALL-TRANSPORT-CHANNEL RESULTS	9
VI. DISCUSSION	11
VII. CONCLUSIONS	14

TITLE AUTHOR SUBJECT ABSTRACT	
DISTRIBUTION STATEMENT SECURITY CLASSIFICATION	
REPORT NUMBER PRICE CODES AVAILABILITY STATEMENTS DISTRIBUTION STATEMENTS	
A	

ANALYSIS OF PROTON TRANSPORT EXPERIMENTS

I. Introduction

As a part of the NRL light ion beam research program¹, experiments on the transport^{2,3} of intense pulsed proton beams have been carried out. The NRL GAMBLE II pulser was used to generate proton beams and the measurement of prompt-gamma rays⁴ was the primary diagnostic for proton transport. The first sequence of shots was made using a large-diameter (4.5 cm) transport channel with a 2.5-cm diameter aperture. The transport of 1-MeV proton beams of a few hundred kiloamperes a distance of one meter with efficiencies approaching 100% was achieved in this channel. A second sequence of shots with a smaller-diameter (1.6 cm) channel with a 1.2-cm diameter aperture was much less efficient in transporting the beam. Analysis of the prompt-gamma measurements to determine proton currents in the transport channel and transport efficiencies is presented in this report.

II. Description of Experiment

The proton beam was generated by a planar pinch-reflex diode⁵ with a 5.7-cm radius cathode. The beam was brought to a narrow-angle focus 25 cm from the diode and injected into a transport channel. The vacuum diode was separated from the low-pressure-gas-filled transport region by a 1.8- μ m thick Kimfol. The proton beam was focused by self B-fields in the 1.9-cm anode-to-Kimfol gap and, after passing through the Kimfol, was ballistically directed toward the focal region. At the expected focus, the beam entered the transport channel which consisted of a wall-stabilized plasma discharge

Manuscript submitted June 24, 1980

typically carrying an externally applied axial current of ~ 50 kA. The B-field from this current was sufficient to confine the injected protons within the larger diameter channel.

The proton beam in the channel was diagnosed by measuring prompt gamma rays⁴ from the $^{19}\text{F}(p,\alpha\gamma)^{16}\text{O}$ reaction. For this diagnostic, Teflon screen targets (50% transparent) were located at the entrance to the channel and one meter into the channel. Two detectors were used to measure prompt gamma rays from these targets as shown in Fig. 1. One detector, which was absolutely calibrated⁶, was located 58 cm from the second target and shielded against radiation from the diode and first target. The other detector was located behind a concrete wall and was equidistant from both targets. The wall differentially shields the diode bremsstrahlung and improves the signal-to-bremsstrahlung ratio for viewing the first target. Measured signals from these two detectors are displayed in Fig. 2. These responses indicate that the inside detector measured signals from the second target while the outside detector recorded signals from both targets. The outside-detector signals are separated in time by the transit of protons from the first to the second target. The detector behind the concrete wall was calibrated absolutely by comparing its response from the second target with that obtained with the inside detector.

For a shot with no Teflon targets, the prompt-gamma responses are given by the dashed curves in Fig. 2. On this background shot, sufficient energy was transported to spall an aluminum plate at the end of the transport system. A small bremsstrahlung signal was measured on the outside detector. The inside detector recorded no bremsstrahlung but did record a small signal probably due to residual Teflon deposited in the transport system from

previous shots. If the apparatus was not cleaned carefully between shots, this background was significantly larger.

Protons injected into the transport channel propagate in the magnetic field associated with the discharge current. The channel is essentially a z-pinch, a radial implosion followed by damped radial oscillations. The confinement of the protons to the channel depends on the radial profiles of the magnetic field, current, and particle density in the channel. These qualities are rapidly varying functions of time and are not known. For the present analysis, the channel is assumed to be of uniform particle and current density and constant in time for the duration of the beam pulse.

Measured prompt-gamma responses were compared to responses calculated using the ion current and proton energy measured on each shot. The charged-particle current incident on the Kimfol was measured with a Rogowski coil. The proton energy was taken to be the voltage determined by correcting the measured diode voltage for inductive effects in the diode and for classical energy loss in the Kimfol. The ion current, presumed to be entirely protons, and the proton energy were combined with the energy dependence of the $^{19}\text{F}(p,\alpha\gamma)^{16}\text{O}$ reaction and the absolute detector sensitivity⁶ to give the expected prompt-gamma response. The energy dependence of this reaction yield is shown in Fig. 3. Corrections for the flight time of protons from the anode to the target were included in the calculations. The shapes and magnitudes of the calculated responses were compared to the measured responses after timing-chain corrections.

III. Large-Transport-Channel Results

Six shots with the large-diameter transport channel were selected for careful analysis. The calculated prompt-gamma responses for these shots are compared with the measured signals in Fig. 4. Here the calculated responses

have been normalized in amplitude to the measured signals. The proton current and energy used for these calculations are also displayed in Fig. 4 for each shot. The current measured on shot 407 was used for shot 406 because that trace was not recorded on shot 406.

The shapes of the calculated responses from the first target agree reasonably well with the measured traces for all the shots except shot 413. Also, the calculated risetimes for responses from the first target agree with the measured traces except for shot 402. The prompt-gamma signals from the first target for shots 402 and 403 were measured at 50 ns/cm and expanded to 20 ns/cm for the comparison in the attached figures. An error of ± 5 ns is inherent in the absolute time scale for these two traces. For shot 413, the calculated response from the first target is narrower in width than the measured trace. The calculated response is narrowed in time due to the peculiar shape of the voltage trace measured on this shot. The narrow peak on the prompt-gamma response is correlated with the narrow peak at the top of the voltage. Explanations for the discrepancy with the measured trace are speculated upon in the discussion (Section VI).

The calculated responses from the second target do not agree with the measured signals in shape or timing. The calculated responses occur too early in time presumably because the proton energy is too high. No energy loss in the focusing region or the transport system has been included in these calculations.

IV. Transport Efficiencies and Energy Losses in the Large Channel

A lower limit on the transport efficiency can be estimated from the ratio of the prompt-gamma signals from the first and second targets. Signals from both targets are recorded with equal sensitivity by the outside detector. The areas of the two peaks in the traces for this detector were used to

evaluate the transport efficiencies given in Table 1. For this evaluation the area of the second peak has been doubled relative to the first peak to correct for the 50% transparent Teflon screen targets. Table 1 also lists the air pressure in the transport channel for each shot. The largest transport efficiency was obtained for 0.5-Torr pressure. At a pressure of 0.12 Torr, the efficiency was reduced to about 20%. These efficiencies are in fact lower limits on the transport efficiency because energy lost by protons in the transport system causes the prompt-gamma signal from the second target to be reduced. The strong energy dependence of this diagnostic is shown in Fig. 3.

To estimate the magnitude of energy losses in these experiments, the average energy of the protons in the transport channel was determined for several shots. The time interval between signals from the two Teflon targets was used to calculate the average proton energy, E_a , in the channel. This energy is compared in Table 2 with the maximum energy of the ions, E_m , after passing through the Kimfol. The difference between E_m and E_a represents an average energy loss and ranges from 100 to 430 keV for these shots. For this comparison, a proton energy extracted from the timing of the maxima of the prompt-gamma responses should correspond to the peak proton energy because this response is strongly energy dependent (see Fig. 3). The average energy losses in Table 2 are larger than one expects from collisional losses in the channel. For example, the classical energy loss for 1.2-MeV protons in 1.5-Torr air is only 50 keV/m. Classical energy losses from the Kimfol to the second target due to the low pressure air in the channel are listed as dE_2 in Table 2. Clearly, energy losses significantly greater than classical collisional losses are reducing the proton energy in these experiments.

Table 1

Large-Channel Transport Results for No Energy Loss

Shot No.	Transport Channel Pressure (Torr)	Minimum Transport Efficiency
402	1.5	0.25
403	1.5	0.12
406	1.5	0.30
407	1.5	0.26
412	0.5	0.47
413	0.28	0.31

Table 2

Energy Loss Estimates

Shot No.	E_m (MeV)	E_a (MeV)	Average Energy Loss (keV)	dE_2 (keV)	ΔE_2 (keV)	dE_1 (keV)
402	0.975	0.88	100	70	300	13
403	1.10	0.93	170	60	--	--
406	1.22	0.96	260	64	--	--
407	1.39	1.01	380	60	600	12
412	1.26	0.93	330	21	500	4
413	1.44	1.01	430	10	700	2

An evaluation of the transport efficiency including energy loss was made for shots 402, 407, 412 and 413. On these shots, efficient transport was observed and all data traces were obtained. For this analysis, the energy loss was assumed to be constant during the beam pulse and was applied directly to the measured voltage to reduce the energy of the protons before time-of-flight corrections thru the focusing and transport sections. The energy loss of the protons after passing through the Kimfol was assumed to consist of a classical energy loss dE due to gas in the channel, and an additional energy loss ΔE to be determined. Subscripts of 1 or 2 will be used on these quantities to denote energy losses from the diode to the first or second Teflon target, respectively. The energy loss of protons from the diode to the Teflon target at the end of the transport system was determined from proton time-of-flight. The energy of the protons after passing through the Kimfol was reduced about an amount $(dE_2 + \Delta E_2)$, and ΔE_2 was adjusted so that the peak of the calculated prompt-gamma signal from the second target agreed in time with the measured signal. Values of dE_2 and ΔE_2 are given in Table 2. An uncertainty of ± 100 keV is assigned to ΔE_2 based on this fitting procedure. The fitting procedure is illustrated in Fig. 6. In all cases the additional energy loss ΔE_2 is much greater than the classical energy loss dE_2 . The energy of protons striking the second target is less than the average energy measured in the transport channel, assuming deceleration during transport. Therefore the energy loss from the Kimfol to the second target is larger than the average-energy-loss estimates in Table 2.

The energy loss of the protons is made up of an energy loss in the region from the diode to the first Teflon target (ΔE_1), and an energy loss in the transport channel between the two targets (ΔE_t), where $\Delta E_1 + \Delta E_t = \Delta E_2$. Both ΔE_1 and ΔE_t are not known, but the sum, ΔE_2 , was determined above.

A range of values for ΔE_t (and hence ΔE_1) is determined by comparing the intensities of measured and calculated prompt-gamma responses. Prompt-gamma responses were calculated for the first target with protons reduced in energy by $(dE_1 + \Delta E_1)$ and for the second target with protons reduced in energy by $(dE_2 + \Delta E_2)$. The ratio for these results was used to correct the minimum transport efficiencies determined previously for no energy loss. The results are presented in Fig. 5 as a function of ΔE_t . Values of dE_1 are given in Table 2. As ΔE_t increases, the transport efficiency increases until an upper-limit of 100% is reached. Over this range, ΔE_t never exceeds 150 keV and is always less than ΔE_1 . For $\Delta E_t = 100$ keV, a likely value, the transport efficiency ranges from 50% to 90%, and ΔE_1 ranges from 200 to 600 keV for these shots.

Only a fraction of the measured ion current is incident on the 2.5-cm diameter Teflon target at the entrance to the transport channel. The fraction of the ion current required to fit the magnitude of the measured prompt-gamma signal from the first target is determined by scaling the measured ion current by the ratio of the measured to calculated prompt-gamma signals. This fraction was determined by integrating the respective signals to eliminate uncertainties due to proton bunching and multiplying by two to correct for the 50% transmission Teflon screen target. This fraction is presented in Fig. 5 as a function of the energy loss in the transport channel, ΔE_t . For less energy loss in the transport channel and more energy loss from the diode to the channel entrance, a larger fraction of the ion current is required to account for the magnitude of the prompt-gamma signal. For $\Delta E_t = 100$ keV, this fraction ranges from 20% to 85% for these shots. Since the measured ion current at peak voltage is about 500 kA for all these

shots (see Fig. 1), currents of 100 to 400 kA at peak voltage were inferred from this analysis.

The inclusion of energy losses in calculating the prompt-gamma responses has minimal effect on the shapes of the calculated responses as illustrated in Fig. 6 for shot 412. The fitting procedure used to determine the energy loss ΔE_2 is shown for the inside detector. If this same energy loss is used for ΔE_1 (i.e. $\Delta E_t = 0$), the timing of the calculated signal from the first target is only slightly delayed because the flight path of protons to the first target is so short.

V. Small-Transport-Channel Results

Measured prompt-gamma signals for two shots with protons injected into the small-diameter transport channel are compared with calculated responses in Fig. 7. These shots were selected because they gave observable transport. Other shots gave unobservable or barely observable transport. The reason for the poor transport in these shots will be discussed later. The proton energy and current used for these calculations are also displayed in Fig. 7. No energy losses have been included in the calculations, and the calculated responses were normalized in amplitude to the measured signals. For shot 419, helium gas was used in the channel instead of air. The channel pressure for each shot is given in Table 3.

The shapes of the calculated responses from the first target compare favorably with the measured traces, but the measured traces occur significantly earlier than the calculated traces. This discrepancy is due to a significant contribution to the first-target signal from diode bremsstrahlung. The measured signals are smaller due to the smaller entrance aperture on the transport channel, and the diode bremsstrahlung is larger in this series of shots so the signal-to-bremsstrahlung ratio is reduced.

The calculated responses from the second target do not agree with the measured signals in shape or absolute time. In fact, for shot 419 the measured response occurs earlier in the time than the calculated response. This suggests that the energy of some protons is greater than the measured diode voltage so that they arrive at the second target earlier in time. One might suspect that this early-time signal is due to protons bombarding a Teflon deposit remaining on the inside walls of the transport channel after previous shots. However, this explanation is unlikely because the channel was carefully cleaned between shots (see Fig. 2).

An analysis including energy loss has not been applied to these small transport channel shots because there are unknown bremsstrahlung contributions to the prompt-gamma signals from the first target and because the proton energy loss from the diode to the second target is poorly determined. Even so, minimum transport efficiencies may be evaluated from the ratio of the measured prompt-gamma signals from the two targets. The results are given in Table 3. These efficiencies are significantly smaller than the results obtained with the larger diameter channel.

Table 3

Small-Channel Transport Results for No Energy Loss

Shot No.	Gas	Transport Channel Pressure (Torr)	Minimum Transport Efficiency
417	Air	0.25	0.06
419	He	1.0	0.09

VI. Discussion

Protons injected into the transport channel propagate in and are confined by the magnetic field produced by the discharge current. Confinement within the channel depends on many factors. If a uniform static discharge current, I , is assumed, then protons entering the channel at angles up to a maximum of θ_m to the channel axis will be confined according to³

$$I = \frac{10^{-3}v(1-\cos\theta_m)}{1-(a/R)^2}$$

where I is in amperes, v is the proton speed in cm/s, R is the channel radius and $a < R$ is the radius of the channel entrance aperture. For 1-MeV protons and the maximum possible injection angle in the present experiments, a current of 58 kA in the large channel or 72 kA in the small channel is required.

In the experiments, typically 50 to 60 kA flowed in the large channel, but only \sim 30 kA flowed in the small channel due to the increased channel resistance and the capacitor bank limitations. In the latter case, the channel current quarter-period rise time was about 15 μ s. It is tempting to conclude that the transport efficiencies observed in the small channel were determined principally by the available discharge current. However, it was found in the experiments that observable transport ceased at the highest current levels in the small channel. Transport efficiency was increased by injecting the beam earlier in the rise of the channel current or by shortening the rise time of the channel current, even though the absolute level of channel current decreased.

These observations point to the necessity for a more realistic interpretation of the beam-channel system. The radial profiles of magnetic field, current, and density in the channel are rapidly varying functions of time and depend on such variables as plasma temperature, gas composition, impurity

contamination from the channel walls, etc. Thus, the transport efficiency depends on a detailed knowledge of the channel properties at the moment of beam injection and of the interaction of the beam-plasma system. We cannot presently obtain this information experimentally because the discharge is difficult to probe without disruption which may effect beam transport. MHD code work simulating the beam-discharge interaction is in progress.⁷ For some channel conditions, MHD instabilities, which can inhibit transport, may grow.⁸ The abrupt loss of transport at higher currents in the small channel suggests this possibility. Future experiments will test the role of instabilities by establishing the channel current on a much faster time scale. Under this condition, the instability growth time before beam injection is reduced.

The observed beam-energy losses cannot be simply explained at present. The results indicate that the energy losses substantially exceed those expected from classical collisional losses in the gas at fill pressure. It is apparent that losses occur both in the region between the anode and the transport channel entrance aperture and within the channel itself. In many cases, the out-of-channel losses are more severe. There are many possible explanations for these losses. In the pinch-reflex diode, the anode foil is vaporized and ionized to some extent by the electron beam. The electrons reflex through this plasma on their way to the pinch region at the anode center. This is a resistive plasma so that a substantial radial voltage drop can occur across this plasma. The energy of ions extracted from this plasma would depend on their point of origin within the plasma and would always be less than or equal to the voltage applied to the diode. Also, the self-inductance of the beam between the anode and the Kimfol extracts energy from the beam. Additionally, there may be losses due to microturbulence in the

gas,⁸ and associated losses due to resistive and hydrodynamic electric fields which develop inside the channel during beam transport.⁷ Furthermore, since a dynamic plasma exists in the transport system, the beam may lose or gain energy from axial electric fields created from plasma contraction or expansion.⁹ This may explain the apparent acceleration of some protons to energies greater than the diode voltage as observed on shot 419. Finally, ions confined to a region close to the axis of the transport channel may sustain enhanced collisional losses if the pinch has compressed the plasma to densities significantly greater than the fill pressure. Wall material brought into the discharge during implosion can also contribute to collisional losses.

The large-diameter-channel measurements indicate that most of the ion beam could be injected into the 2.5-cm diameter aperture and transported. For the small channel, measurements from the first target indicate that less than half of the proton beam is contained within the 1.2-cm diameter aperture. On some shots with the small transport channel, the entrance aperture was increased to 1.6-cm diameter and the first target was removed. Signals from the second target increased by more than the factor-of-two expected by just removing the 50% transmission target. In this case, more protons were injected into the channel and transported. It should be noted that since the voltage and current of the ion beam vary in time, the position of best focus moves axially during the beam pulse. For inertial confinement fusion applications, diodes with improved focusability at long focal lengths are required.³

In the large-transport-channel analysis (Section IV), energy losses from the diode to the transport channel and within the channel itself were assumed constant during the beam pulse. For the reasons described above, it is apparent that the energy loss is not constant. Therefore, it is not

surprising that the shapes of the calculated prompt-gamma responses do not fit the shapes of the measured signals from the second target even though time-of-flight effects are included in the analysis. As a result, the energy analysis in Section IV is a time-averaged approximation as are the magnitudes of the energy losses.

VII. Conclusions

The best transport results were obtained with the large diameter channel. In this channel, transport efficiencies ranging from 33% to 100% were deduced from this analysis. Total proton currents of a few hundred kiloamperes of 1-MeV protons were calculated to be transported a distance of one meter. There is a trade off between proton current and transport efficiency in the interpretation of these measurements. For 100% transport efficiency in the shots analyzed, the current is ≤ 250 kA, but for the smallest transport efficiency (33%) of any of the shots, the current is 300 kA. Energy losses within the transport channel were less than 15% of the maximum proton energy.

References

1. G. Cooperstein, S. A. Goldstein, D. Mosher, R. J. Barker, J. R. Boller, D. G. Colombant, A. Drobot, R. A. Meger, W. F. Oliphant, P. F. Ottinger, F. L. Sandel, S. J. Stephanakis and F. C. Young, "NRL Light Ion Beam Research for Inertial Confinement Fusion," 5th Workshop on Laser Interaction and Related Plasma Phenomena, Rochester, N.Y., 1979.
2. F. L. Sandel, F. C. Young, S. J. Stephanakis, W. F. Oliphant, G. Cooperstein, S. A. Goldstein, and D. Mosher, *Bull. Am. Phys. Soc.* 24, 1031 (1979); and F. C. Young, F. L. Sandel, S. J. Stephanakis, P. G. Blauner, W. F. Oliphant, G. Cooperstein, S. A. Goldstein and D. Mosher, *ibid.* 24, 1031 (1979).
3. D. Mosher, G. Cooperstein, S. A. Goldstein, D. G. Colombant, P. F. Ottinger, F. L. Sandel, S. J. Stephanakis and F. C. Young, "Transport and Bunching of Light Ion Beams for Pellet Fusion," 3rd Inter. Conf. on High Power Electron and Ion Beam Res. and Tech., Novosibirsk, USSR, 1979.
4. J. Golden, R. A. Mahaffey, J. A. Pasour, F. C. Young, C. A. Kapetanacos, *Rev. Sci. Instrum.* 49, 1384 (1978).
5. D. Mosher, G. Cooperstein, S. J. Stephanakis, S. A. Goldstein, D. G. Colombant and R. Lee, "Intense Focussed Ion Beams and Their Interaction with Matter," 2nd Int. Conf. on High Power Electron and Ion Beam Res. and Tech., Cornell University, Ithaca, N.Y., 1977, p. 257; and S. A. Goldstein, G. Cooperstein, R. Lee, D. Mosher and S. J. Stephanakis, *Phys. Rev. Lett.* 40, 1504 (1978).
6. F. C. Young, F. Oliphant, S. J. Stephanakis, and A. K. Knudson, "Absolute Calibration of a Prompt Gamma Ray Detector for Intense Bursts of Protons," NRL Memorandum Report 4171, March, 1980.
7. D. G. Colombant and S. A. Goldstein, "Scaling Laws for Ion Beam Losses in Plasma Channels," Conf. Record-1980 IEEE Inter. Conf. on Plasma Science, Madison Wisconsin, 1980, p. 37.
8. P. F. Ottinger, D. Mosher and Shyke A. Goldstein, *Phys. Fluids* 22, 332 (1979).
9. S. A. Goldstein and D. A. Tidman, "Particle Beam Acceleration in Magnetized Moving Plasma," Conf. Record-1980 IEEE Inter. Conf. on Plasma Science, Madison, Wisconsin, 1980, p. 96.

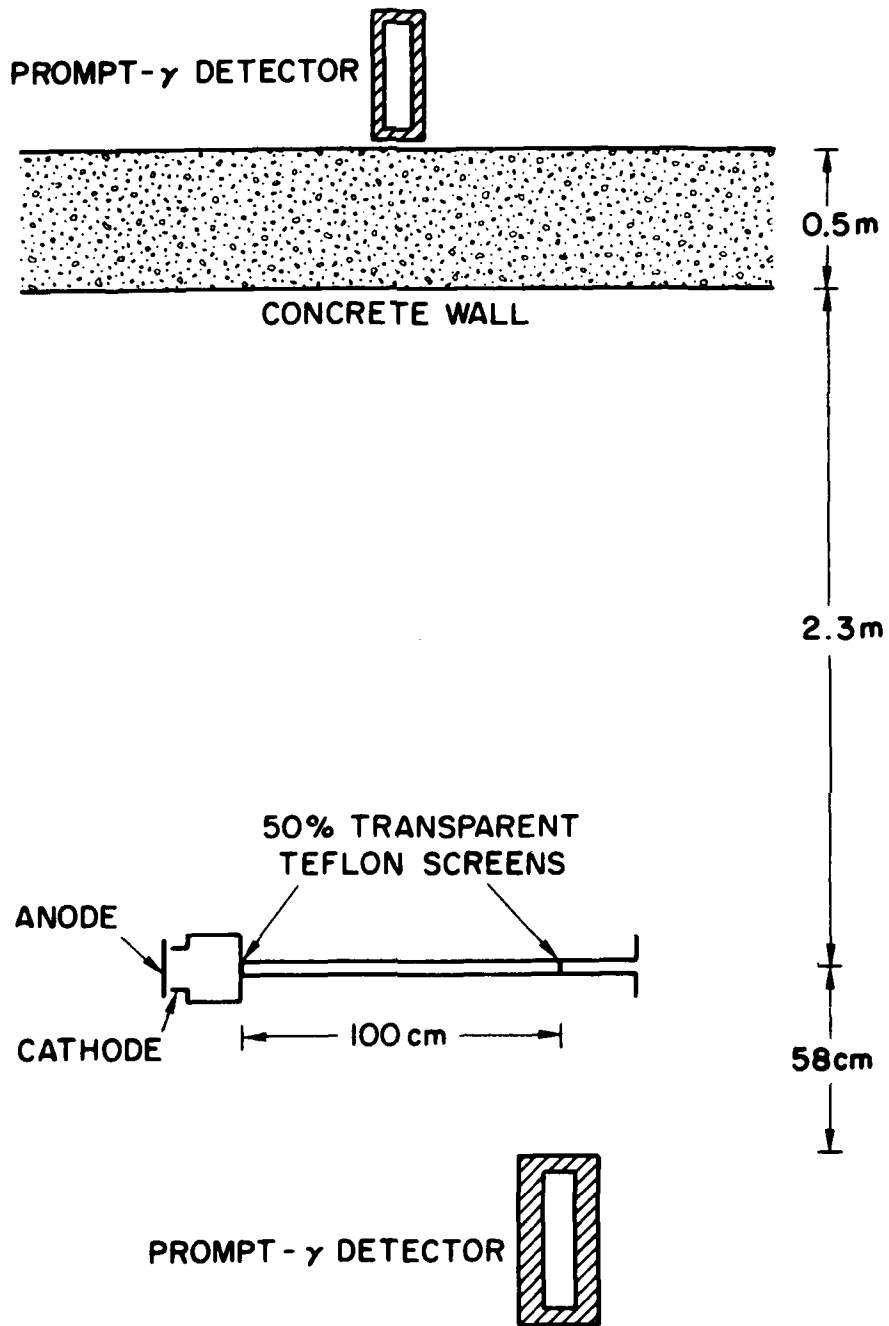


Fig. 1 — Experimental arrangement of the prompt-gamma detectors for the transport experiments.

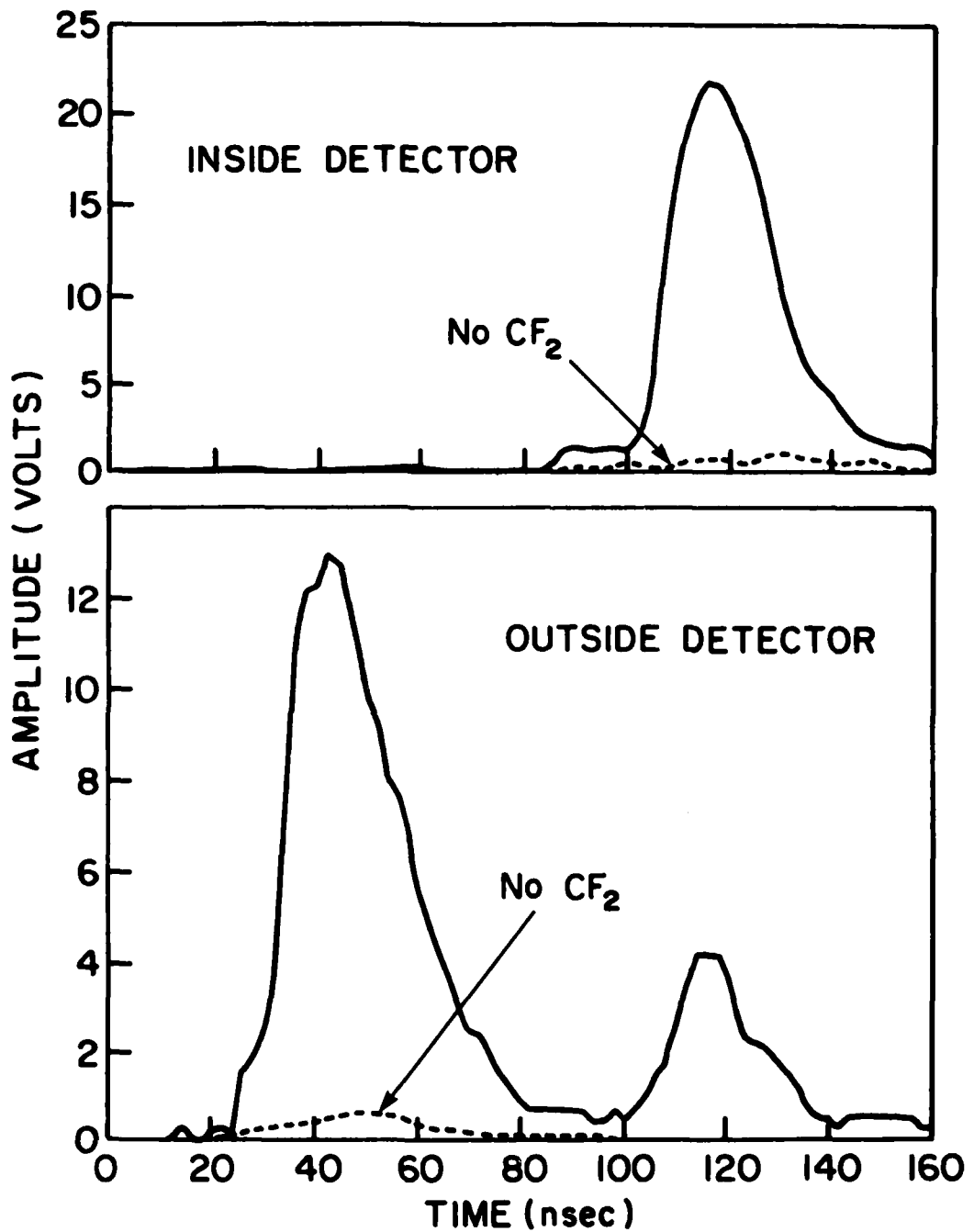


Fig. 2 - Measured traces from the prompt-gamma detectors for Shot 412 with Teflon targets (solid line) and for Shot 411 without Teflon targets (dashed line).

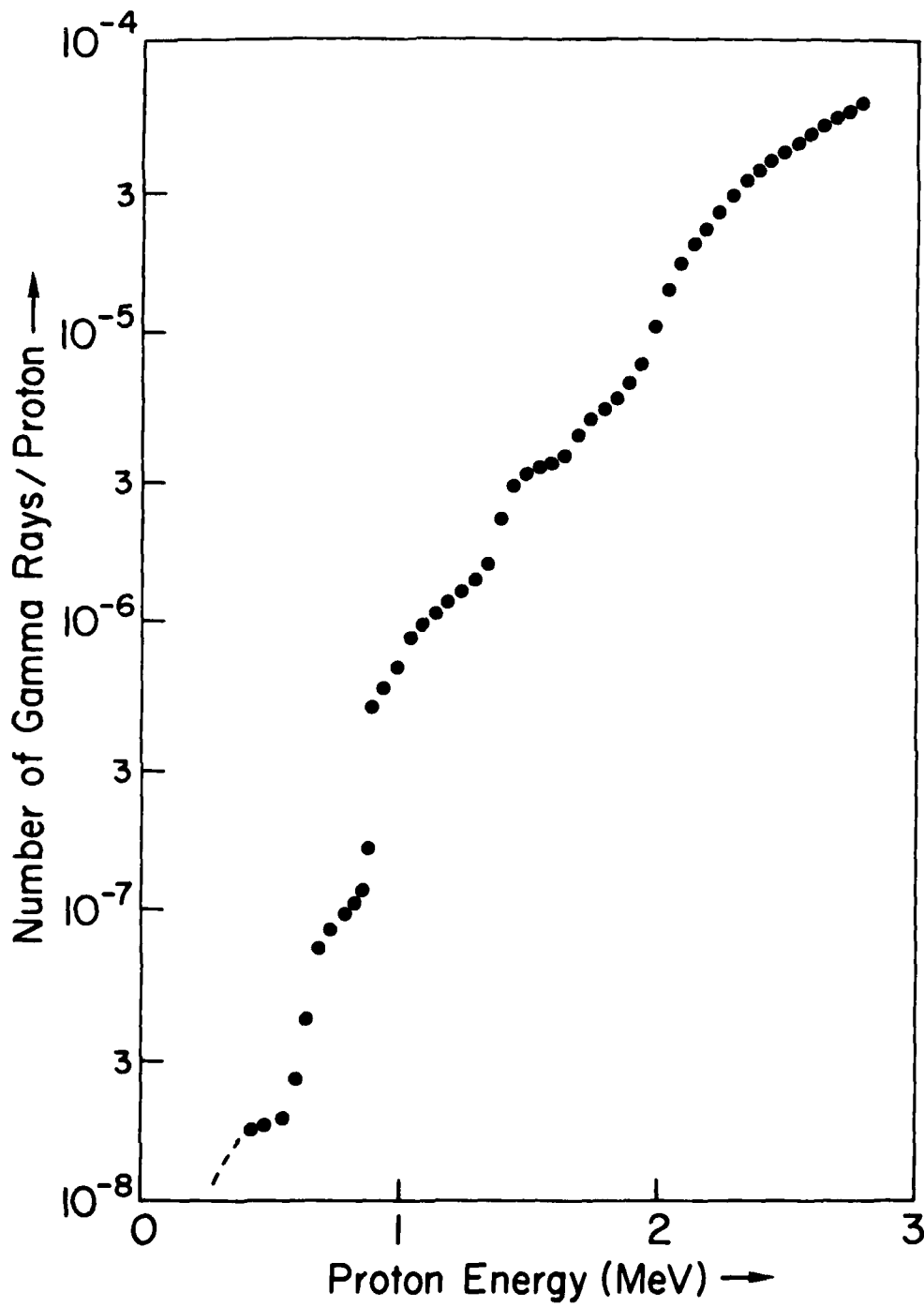


Fig. 3 - Measured thick-target yield for the $^{19}\text{F}(p,\gamma)^{16}\text{O}$ reaction on a Teflon target.

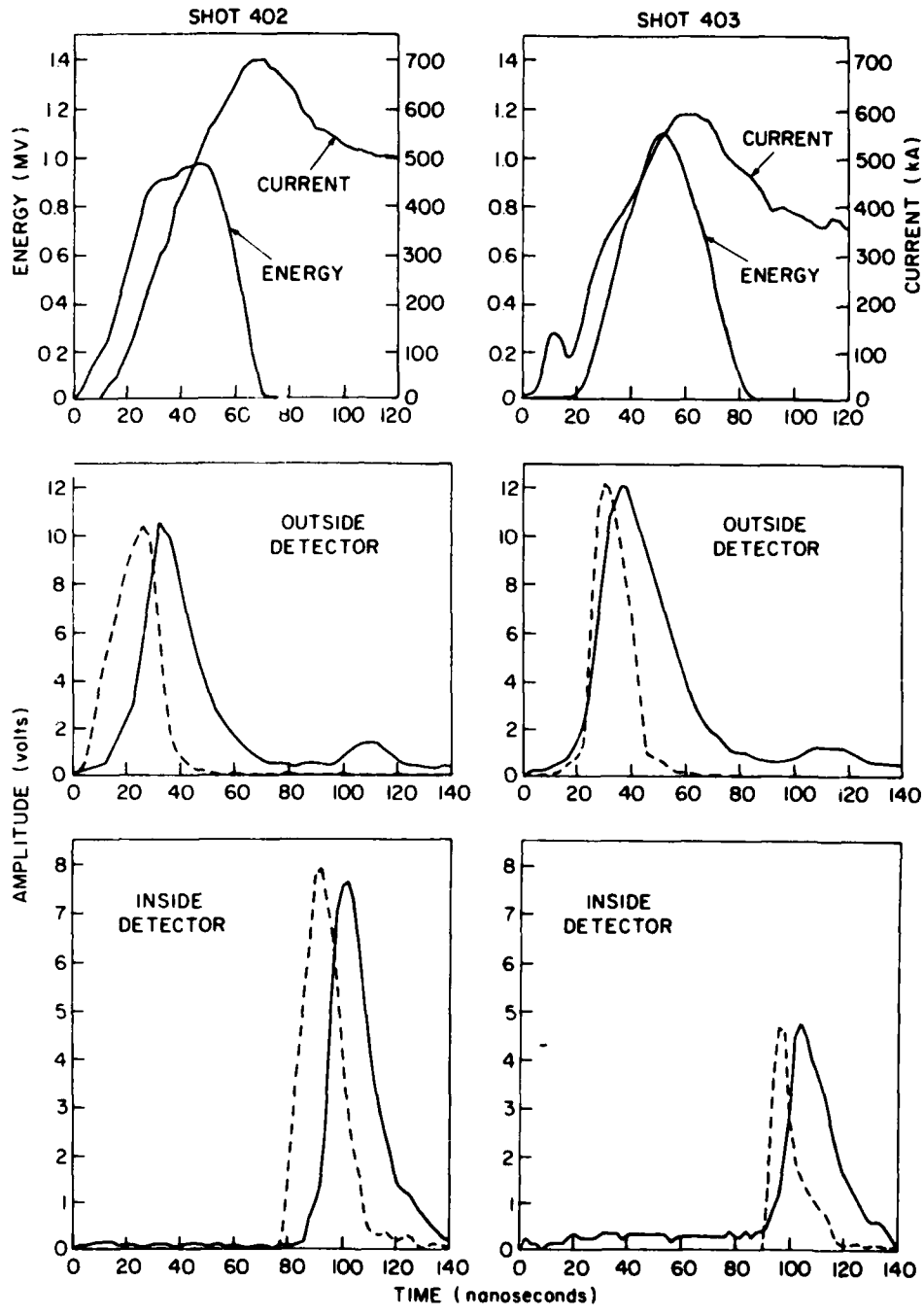


Fig. 4(a) — A comparison of measured (solid line) and calculated (dashed line) prompt-gamma responses for Shots 402 and 403 with the large diameter transport channel. The calculated responses are normalized in amplitude to the measured signals. Also, the proton energy and current which were used to calculate the prompt-gamma responses are displayed. No energy losses are included in these calculations.

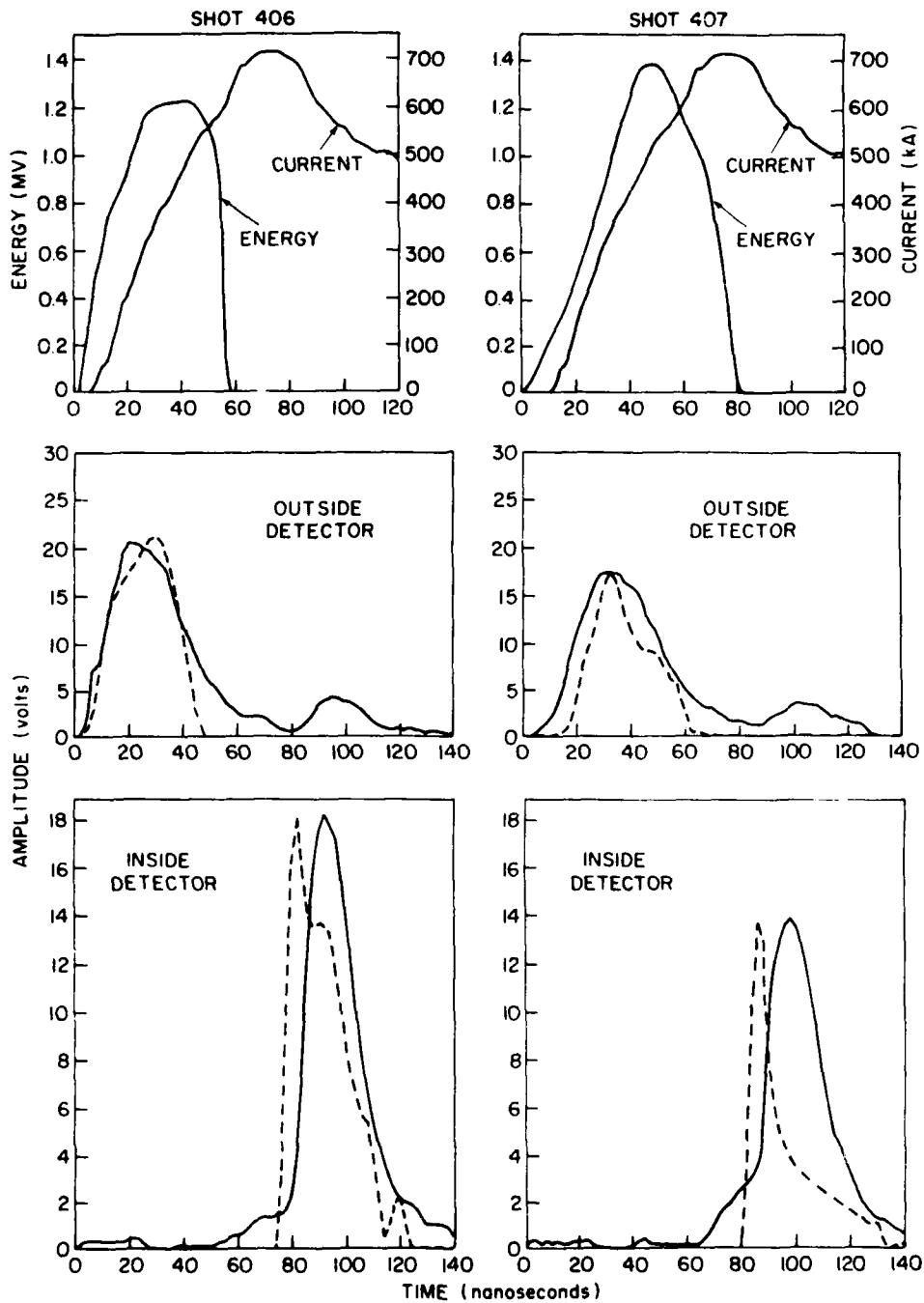


Fig. 4(b) — A comparison of measured (solid line) and calculated (dashed line) prompt-gamma responses for Shots 406 and 407 with the large diameter transport channel. The calculated responses are normalized in amplitude to the measured signals. Also, the proton energy and current which were used to calculate the prompt-gamma responses are displayed. No energy losses are included in these calculations.

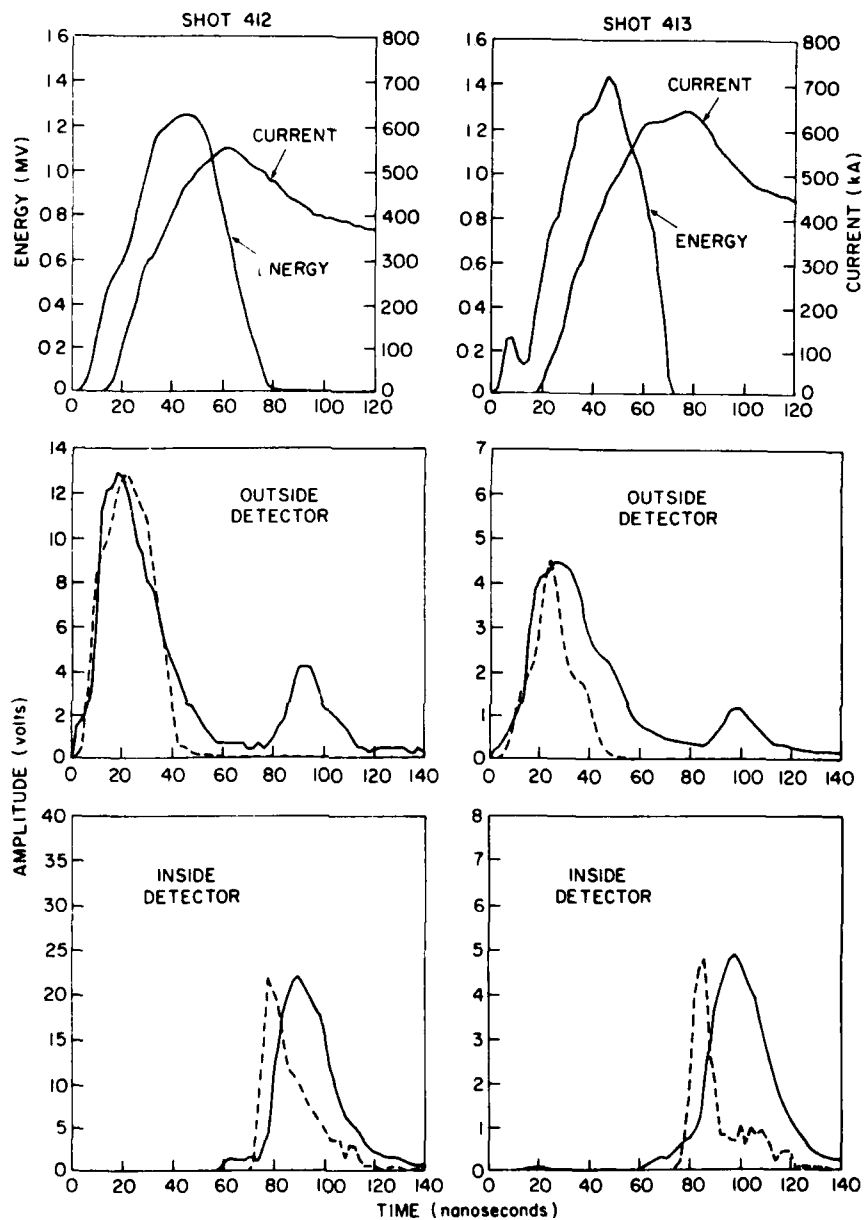


Fig. 4(c) — A comparison of measured (solid line) and calculated (dashed line) prompt-gamma responses for Shots 412 and 413 with the large diameter transport channel. The calculated responses are normalized in amplitude to the measured signals. Also, the proton energy and current which were used to calculate the prompt-gamma responses are displayed. No energy losses are included in these calculations.

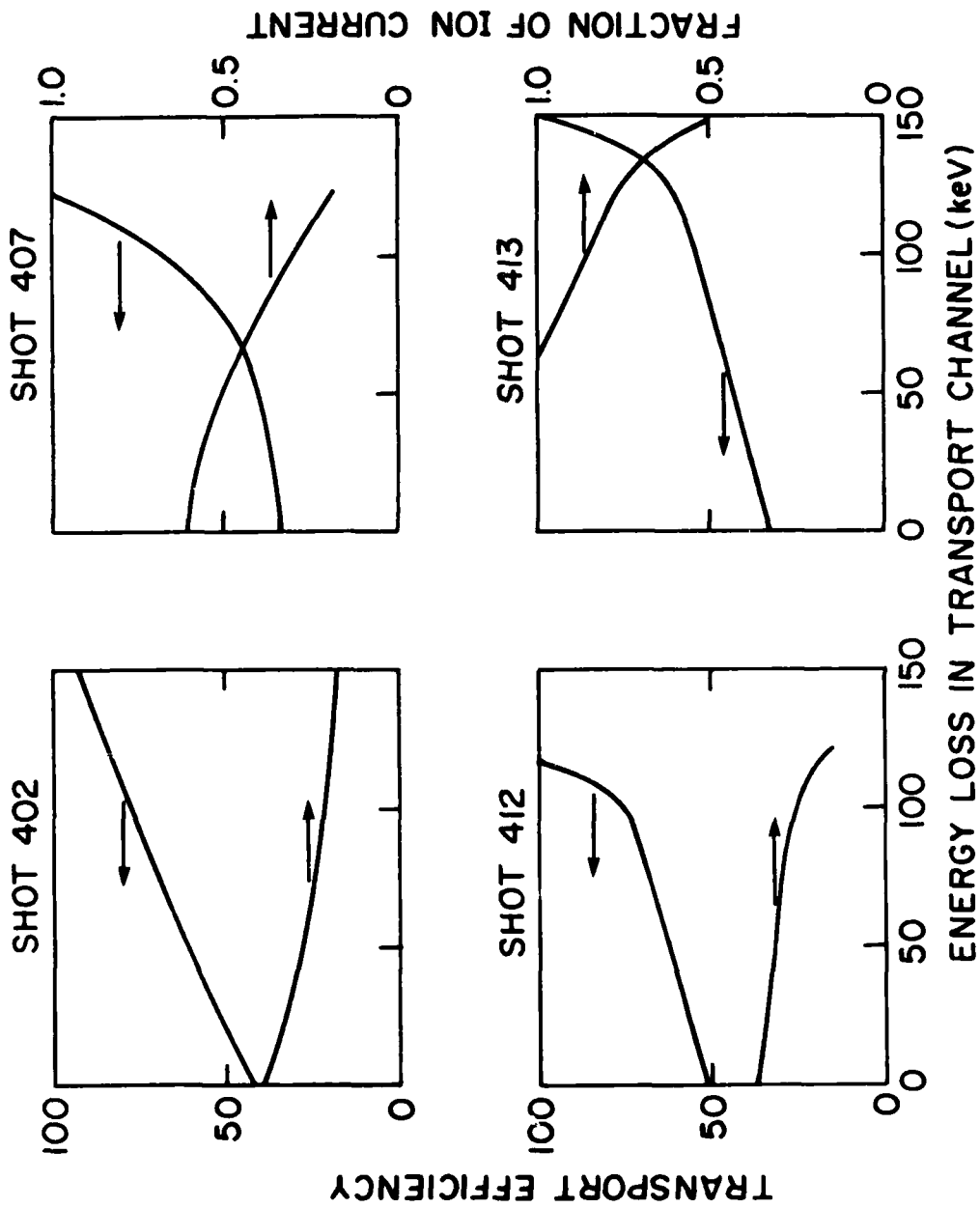


Fig. 5 - Transport efficiencies determined with energy loss included in the analysis. The fraction of ion current required to fit the magnitude of the prompt-gamma response is also given as a function of the energy loss in the transport channel.

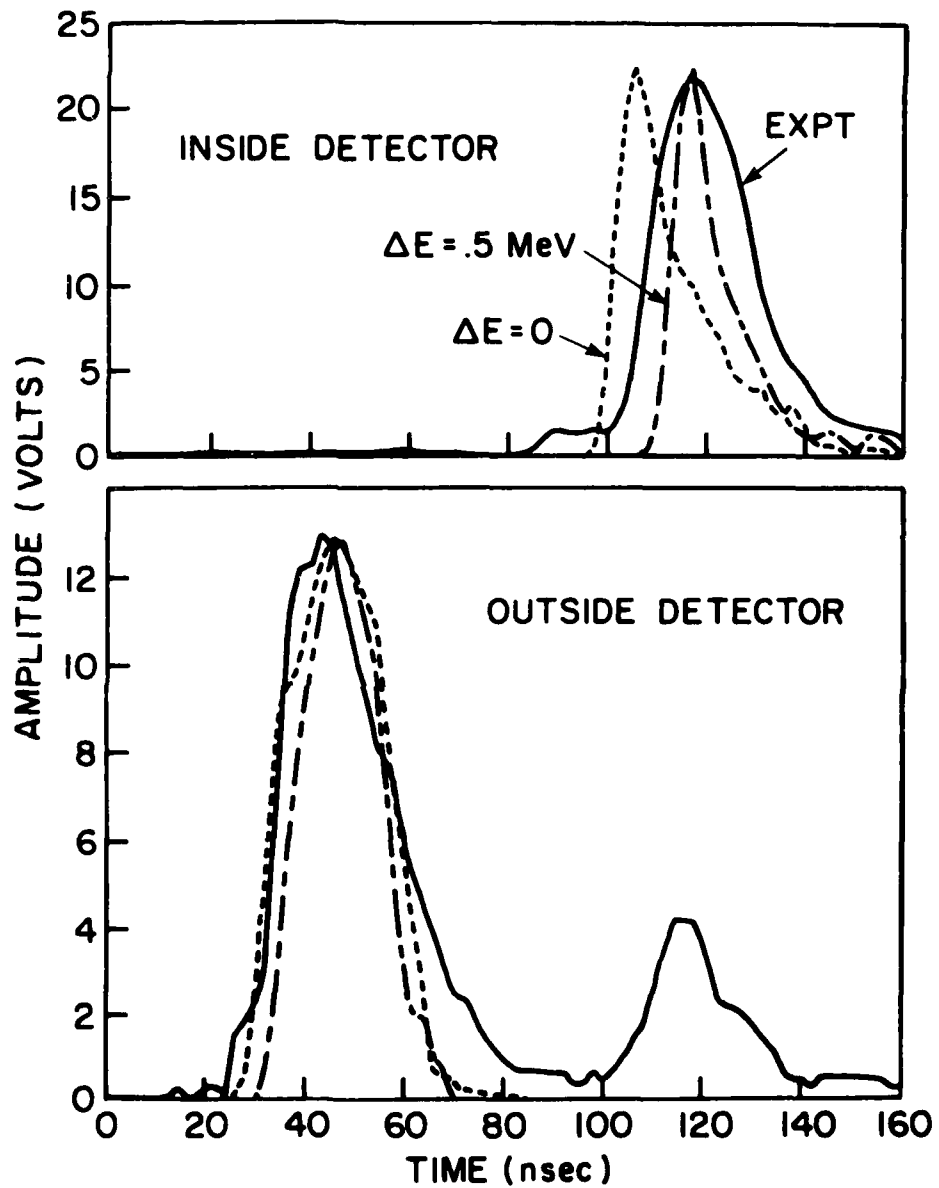


Fig. 6 -- A comparison of measured (solid line) and calculated prompt-gamma responses without energy loss (short dashed line) and with 500-keV energy loss (short-long dashed line) for both prompt-gamma detectors. The measured traces correspond to Shot 412.

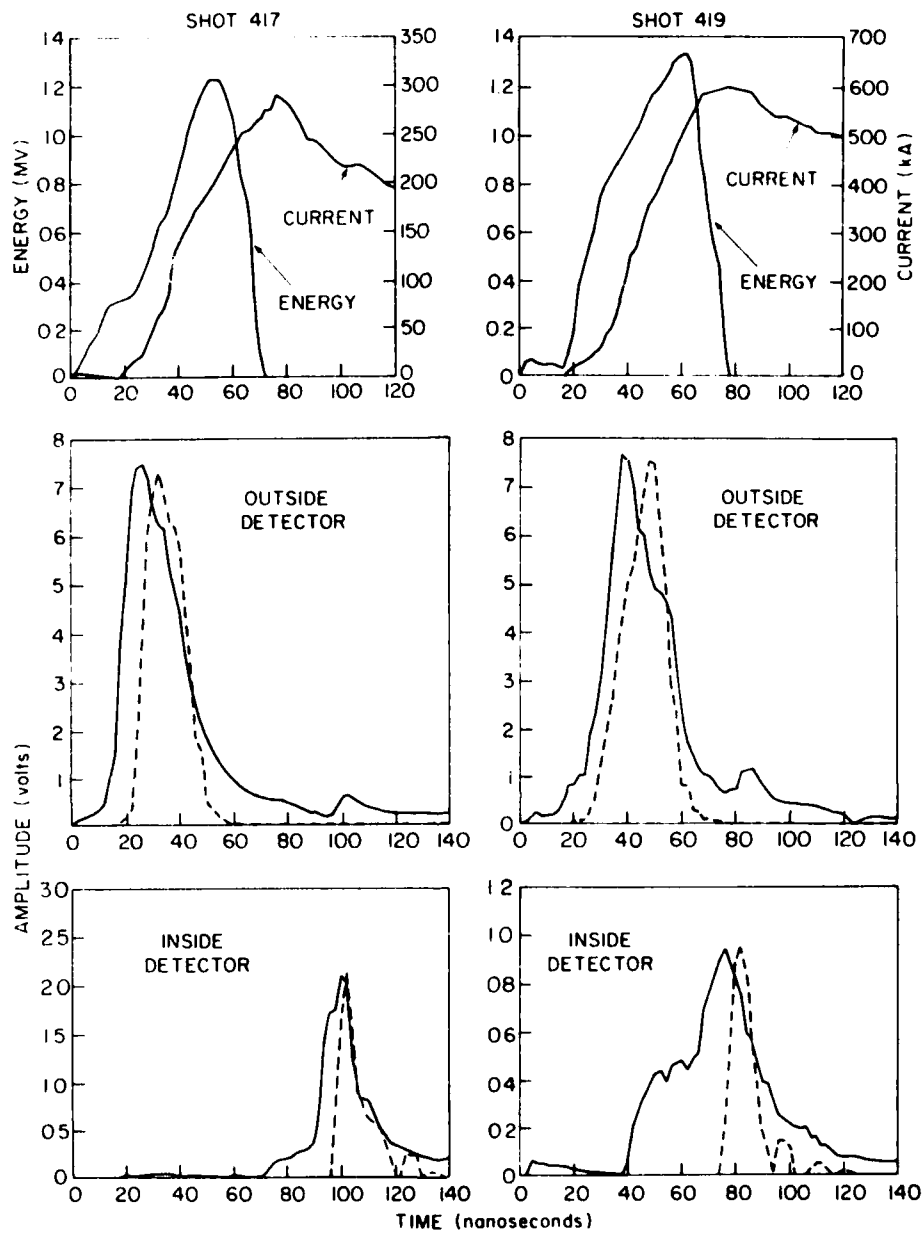


Fig. 7 — A comparison of measured (solid line) and calculated (dashed line) prompt-gamma responses for the small diameter transport channel (Shots 417 and 419). The proton energy and current which were used to calculate the prompt-gamma responses are also displayed. The calculated responses are normalized in amplitude to the measured signals. No energy losses were included in these calculations.

DISTRIBUTION LIST

Air Force Weapons Laboratory, AFSC
Kirtland AFB
Albuquerque, NM 87117

Attn: J. Darrah 1 copy

Argonne National Laboratory
9700 South Cass Avenue
Argonne, Illinois 60439

Attn: R. J. Martin 1 copy
G. R. Magelssen 1 copy

Brookhaven National Laboratory
Upton, NY 11973

Attn: A. F. Maschke 1 copy

Cornell University
Ithaca, NY 14850

Attn: R. N. Sudan 1 copy
D. A. Hammer 1 copy

Harry Diamond Laboratory
Aldelphi, MD 20783

Attn: S. Graybill 1 copy

Director
Defense Nuclear Agency
Washington, DC 20305

Attn: R. L. Gullickson (RAEV) 1 copy
J. Z. Farber (RAEV) 1 copy

Defense Technical Information Center
Cameron Station
5010 Duke Street
Alexandria, VA 22314

12 copies

Grumman Aerospace Corporation
Bethpage, NY 11714

Attn: P. Suh 1 copy

JAYCOR, Inc.
205 S. Whiting Street
Alexandria, VA 22304

Attn: D. A. Tidman 1 copy
R. Hubbard 1 copy
J. Guillory 1 copy

JAYCOR, Inc.
1401 Camino Del Mar
Del Mar, CA 92014

Attn: E. Wenaas 1 copy

JAYCOR, INC.
300 Unicorn Park Drive
Woburn, MA 01801

Attn: H. Linnerud 1 copy

Lawrence Livermore Laboratory
P. O. Box 808
Livermore, CA 94550

Attn: R. J. Briggs 1 copy
R. O. Bangerter 1 copy
J. H. Nuckolls 1 copy
S. S. Yu 1 copy
E. P. Lee 1 copy

Los Alamos Scientific Laboratory
P. O. Box 1663
Los Alamos, NM 87545

Attn: R. B. Perkins 1 copy
L. E. Thode 1 copy
D. B. Henderson 1 copy

Maxwell Laboratories, Inc.
9244 Balboa Avenue
San Diego, CA 92123

Attn: A. C. Kolb 1 copy
P. Korn 1 copy
J. Pearlman 1 copy
R. W. Clark 1 copy

Mission Research Corporation
735 State Street
Santa Barbara, CA 93101

Attn: C. L. Longmire 1 copy

Mission Research Corporation
1400 San Mateo Blvd. SE
Albuquerque, NM 87108

Attn: B. B. Godfrey 1 copy

National Bureau of Standards
Washington, DC 20234

Attn: J. Leiss 1 copy

National Technical Information Service
U. S. Department of Commerce
5285 Port Royal Road
Springfield, VA 22161

24 copies

National Science Foundation
Mail Stop 19
Washington, DC 20550

Attn: D. Berley 1 copy
R. M. Sinclair 1 copy

Naval Research Laboratory
Attn: Name/Code
Washington, DC 20375

Addressee:

Code 2628 - TIC-Distribution 25 copies
Code 6020 - J. Boris 1 copy
Code 6682 - D. Nagle 1 copy
Code 4700 - T. Coffey 25 copies
Code 4707 - J. Davis 1 copy
Code 4730 - S. Bodner 1 copy
Code 4740 - V. Granatstein 1 copy
Code 4760 - B. Robson 1 copy
Code 4761 - C. Kapetanakos 1 copy
Code 4770 - Branch Head 1 copy
Code 4771 - F. Young 74 copies

Naval Research Laboratory (continued)
Attn: Name/Code
Washington, DC 20375

Addressee:
Code 4771 - D. Mosher 10 copies
Code 4773 - G. Cooperstein 10 copies
Code 4770 - S. Stephanakis 10 copies
Code 4790 - M. Lampe 1 copy
Code 4790 - I. Haber 1 copy
Code 4790 - D. Colombant 1 copy

Physics International Co.
2700 Merced Street
San Leandro, CA 94577

Attn: S. J. Putnam 1 copy
A. J. Toepfer 1 copy
P. W. Spence 1 copy
J. Benford 1 copy
R. Genuario 1 copy

B. Bernstein 1 copy
E. B. Goldman 1 copy

R & D Associates
P. O. Box 9695
Marina Del Rey, CA 90291

Attn: E. Martinelli 1 copy
M. Grover 1 copy

Sandia Laboratories
P. O. Box 5800
Albuquerque, NM 87115

Attn: G. Yonas 1 copy
G. W. Kuswa 1 copy
J. R. Frecman 1 copy
D. J. Johnson 1 copy
P. S. Miller 1 copy
J. P. Vandevender 1 copy
S. Humphries 1 copy

Stanford University
SLAC
P. O. Box 4349
Stanford, CA 94305

Attn: W. B. Herrmannsfeldt 1 copy

Systems, Science and Software
P. O. Box 1620
La Jolla, CA 92038

Attn: A. Wilson

1 copy

University of California
Lawrence Livermore Laboratory
Berkeley, Ca 94720

Attn: D. Keefe

1 copy

University of California
Irvine, CA 92664

Attn: G. Benford
N. Rostoker

1 copy

1 copy

U. S. Department of Energy
P. O. Box 62
Oak Ridge, TN 37830

50 copies

U. S. Department of Energy
Division of Inertial Fusion
Washington, DC 20545

Attn: G. Canavan
T. F. Godlove

2 copies

1 copy

University of Illinois
Urbana, IL 61801

Attn: G. H. Miley
J. T. Verdeyen

1 copy

1 copy

University of Rochester
Laboratory of Laser Energetics
River Station, Hopeman 110
Rochester, NY 14627

Attn: M. J. Lubin

1 copy

Bhabha Atomic Research Centre
Bombay - 400085, India

Attn: B. K. Godwal 1 copy
A. S. Paithankar 1 copy

CEA, Centre de Etudes de Lemeil
B. P. 27
94190 Villeneuve, Saint George
France

Attn: A. Bernard 1 copy
A. Jolas 1 copy

CEA, Centre de Etudes de Valduc
P. B. 14
21120 Is-sur-Tille
France

Attn: C. Patou 1 copy
C. Peugnet 1 copy
M. Roche 1 copy
N. Camarcat 1 copy
C. Bruno 1 copy
J. Barbaro 1 copy

Ecole Polytechnique
Labo. PMI
91128 Palaiseau Cedex
France

Attn: H. Doucet 1 copy
J. M. Buzzi 1 copy

Institute of Laser Engineering
Osaka University
Yamadakami
Suita
Osaka 565, Japan

Attn: S. Nakai 1 copy
K. Imasaki 1 copy

Institut d'Electronique Fondamentale
Universite' Paris XI-Bat. 220
F91405 Orsay
France

Attn: G. Gautherin 1 copy

Institut Fur Neutronenphysik
un Reaktortechnik
Postfach 3640
Kernforschungszentrum
D-7500 Karlsruhe 1
West Germany

Attn: H. N. Karow 1 copy
W. Schmidt 1 copy

Instituto De Investigaciones Cientificas Y Technicas
De Las Fuerzas Armadas
Aufriategui y Varela
V. Martelli 1603
Pcia Bs. As. - R. Argentina

Attn: N. B. Camusso 1 copy

Institute of Atomic Energy
Academia Sinica - Peking
People's Republic of China

Attn: R. Hong 1 copy

Max-Planck-Institut fur Plasmaphysik
8046 Garching bei Munchen
West Germany

Attn: R. Lengyel 1 copy

Physical Research Laboratory
Navrangpura
Ahmedabad- 380009- India

Attn: V. Ramani 1 copy

Shivaji University
Kolhapur, India

Attn: L. N. Katkan 1 copy

Weizmann Institute of Science
Rehovot, Israel

Attn: A. E. Blaugrund 1 copy
Z. Zinamon 1 copy
E. Nardi 1 copy